Lithographically Patterned Electrodeposition of Gold, Silver, and Nickel Nanoring Arrays with Widely Tunable Near-Infrared Plasmonic Resonances

Aaron R. Halpern and Robert M. Corn*

Department of Chemistry, University of California-Irvine, Irvine, California 92697, United States

ABSTRACT A novel low-cost nanoring array fabrication method that combines the process of lithographically patterned nanoscale electrodeposition (LPNE) with colloidal lithography is described. Nanoring array fabrication was accomplished in three steps: (i) a thin (70 nm) sacrificial nickel or silver film was first vapor-deposited onto a plasma-etched packed colloidal monolayer; (ii) the polymer colloids were removed from the surface, a thin film of positive photoresist was applied, and a backside exposure of the photoresist was used to create a nanohole electrode array; (iii) this array of nanoscale cylindrical electrodes was then used for the electrodeposition of gold, silver, or nickel nanorings. Removal of the photoresist and sacrificial metal film yielded a nanoring array in which all of the nanoring dimensions were set independently: the inter-ring spacing was fixed by the colloidal radius, the radius of the nanorings was controlled by the plasma etching process, and the width of the nanorings was controlled by the electrodeposition process. A combination of scanning electron microscopy (SEM) measurements and Fourier transform near-infrared (FT-NIR) absorption spectroscopy were used to characterize the nanoring arrays. Nanoring arrays with radii from 200 to 400 nm exhibited a single strong NIR plasmonic resonance with an absorption maximum wavelength that varied linearly from 1.25 to 3.33 μm as predicted by a simple standing wave model linear antenna theory. This simple yet versatile nanoring array fabrication method was also used to electrodeposit concentric double gold nanoring arrays that exhibited multiple NIR plasmonic resonances.

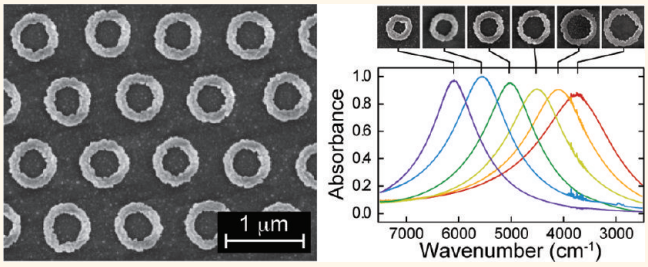

KEYWORDS: nanoring · electrodeposition · nanosphere lithography · backside exposure · plasmonic

Among the panoply of nanoscale objects that have been assembled into ordered arrays on surfaces, nanoscale toroidal rings or "nanorings" are increasingly popular structures that exhibit unique optical, electronic, and magnetic properties with a number of novel technological applications.[1] Some examples include (i) gold or silver nanoring arrays that exhibit strong localized plasmonic resonances with applications in biosensors,[2−6] metamaterials,[7−9] and optical devices,[10,11] (ii) cobalt, iron, or nickel magnetic nanoring arrays that exhibit unique flux closure states with potential applications in magnetic storage,[12−18] and (iii) CdSe, InGaS, or GaN semiconductor nanorings that exhibit unique electronic states for optoelectronic devices.[19−21] A variety of theoretical approaches including Mie theory,[22] plasmon hybridization,[23,24] Green's tensor,[25] and finite-difference time-domain (FDTD) numerical analysis[26] have been used to calculate the electronic structure, plasmonic resonances, and local electromagnetic fields associated with nanorings. A key advantage of the nanorings is that their optical properties can be systematically tuned by varying the ring radius and thickness. To that end, it is vitally important to develop novel methods for fabricating low-cost nanoring arrays from a wide variety of materials with complete control over the nanoring dimensions and array spacing.

One successful and inexpensive method for making nanoring arrays is colloidal

* Address correspondence to rcorn@uci.edu.

Received for review December 18, 2012 and accepted January 18, 2013.

Published online January 18, 2013
10.1021/nn3058505

lithography (also known as nanosphere lithography).[27,28] Vapor deposition of a metallic thin film onto or underneath either a dilute colloidal monolayer or a close-packed self-assembled colloidal monolayer has been used to make a variety of nanoscale objects and arrays (*e.g.*, nanotriangles,[27] nanodisks,[29,30] nanorings,[22,28] and nanocrescents[31,32]). These templated methods cannot attain the precision or complexity of a serial write process such as electron beam lithography (EBL),[33−37] but can rapidly produce nanoring arrays on large length scale (cm^2 or greater) at low cost. A common fabrication approach is to use an argon plasma to sputter metal into the shadowed region of colloidal particles to form a nanoring array.[3,26,38] This technique is capable of forming nanorings down to 60 nm in radius, but has limited control over the ring width. Related methods such as edge spreading lithography,[39,40] evaporation induced self-assembly,[19,41,42] shadow nanosphere lithography,[8,12] and nanoimprint lithography,[2,43,44] have also been used to fabricate nanoring arrays.

Another successful, large area technique for the fabrication of nanoscale arrays is the process of lithographically patterned nanoscale electrodeposition (LPNE).[45,46] In this methodology, a patterned metal thin film sandwiched between an inert substrate and a patterned photoresist layer is used to create a series of recessed nanoband electrodes for nanowire electrodeposition. The LPNE process can create continuous nanowires up to centimeters in overall length in patterns determined by the photoresist layer; the resultant nanowires have a height controlled by the metal film thickness down to 5 nm, and a width controlled by the amount of charge passed during electrodeposition down to 11 nm.[46] A wide variety of materials have been deposited as nanowires by LPNE, including metals (Au, Ag, Bi, Pd, Pt),[47] semiconductors (PbTe, CdSe),[48,49] and a conducting polymer (PEDOT).[50]

In this paper, we combine these two processes, colloidal lithography and LPNE, to create a novel low-cost method for the lithographically patterned electrodeposition of nanoring arrays over large areas. The nanoring arrays are fabricated in three steps: (i) first, a thin (70 nm) sacrificial Ni or Ag film was vapor-deposited onto a plasma-etched packed colloidal monolayer; (ii) the polymer colloids were then removed from the surface to create a nanohole array,[51−53] a thin film of positive photoresist was applied, and a backside exposure of the photoresist was then used to create a nanohole electrode array; and (iii) this array of nanoscale cylindrical electrodes was then used for the electrodeposition of a gold, silver, or nickel nanorings. The photoresist and sacrificial metal film were subsequently removed to reveal a nanoring array in which all dimensions were set independently: the inter-ring spacing was fixed by the colloidal radius, the radius of the nanorings was controlled by the plasma etching process, and the width of the nanorings was controlled by the amount of charge passed during the electrodeposition process. A combination of SEM measurements and Fourier transform near-infrared (FT-NIR) absorption spectroscopy were used to characterize the nanoring arrays. All of the nanoring arrays exhibited a strong tunable near-infrared plasmonic absorption band from 8000 to 3000 wavenumbers. Finally, to show the versatility of this LPNE process, a concentric double gold nanoring array with two NIR plasmonic absorption bands was fabricated.

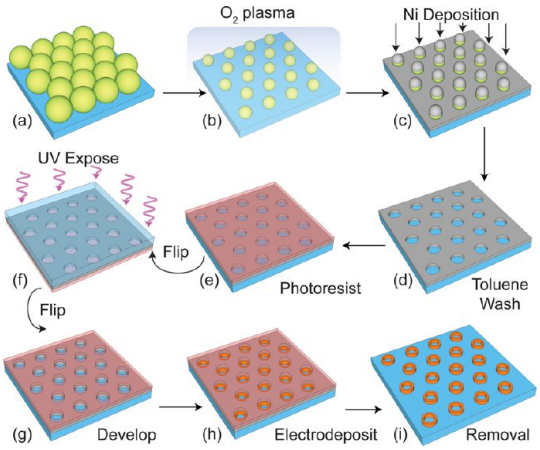

Figure 1. Nanoring fabrication process schematic. (a) A self-assembled colloidal monolayer was formed and (b) etched under O_2 plasma. (c) Ni (or Ag) was evaporated on top and (d) the colloidal monolayer was dissolved in toluene revealing a nanohole array. (e) A photoresist layer was spin coated on top, and (f) backside exposed through the nanohole array. (g) The photoresist was developed and (h) a metal was electrodeposited inside each nanohole. (i) Finally, the sacrificial electrode was selectively removed.

RESULTS AND DISCUSSION

Nanoring Array Fabrication Methodology. Our method for the electrodeposition of nanoring arrays combines the process of LPNE with colloidal lithography. It builds on the previous works of Menke *et al.* for nanowire fabrication by LPNE,[45] and Ctistis *et al.* for creating nanohole arrays from an ordered colloidal template.[51] The process is shown schematically in Figure 1, where it is divided into nine steps: (a) A colloidal monolayer was formed by spin coating a polystyrene bead solution (1 or 0.5 μm in diameter) onto a hydrophilic glass surface. The glass substrates were 2.5 cm × 2.5 cm and rendered hydrophilic by exposure to an oxygen plasma. An optical microscope was used to observe the formation of the monolayer, and the parameters for spin coating were adjusted as necessary. (b) The colloid monolayer was dry etched in an O_2 plasma to reduce the bead diameters. (c) The sample was coated with a 70 nm Ni (or Ag) sacrificial metallic thin film by thermal vapor deposition. (d) In a lift off step, the beads and their metal overcoat were removed with toluene, revealing the nanohole array. (e) The array was

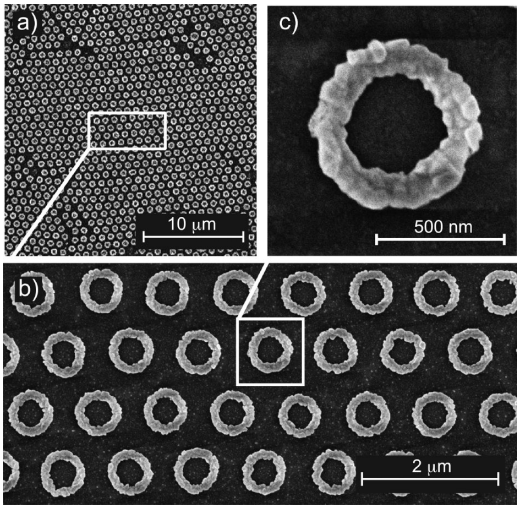

Figure 2. SEM images of Au nanorings created from 1 μm colloids. (a) Low magnification image of a domain of ordered nanorings. (b) Increased magnification of nanorings with outer radius = 330 $\pm$ 5 nm and width = 135 $\pm$ 4 nm, and (c) highest magnification of a single ring.

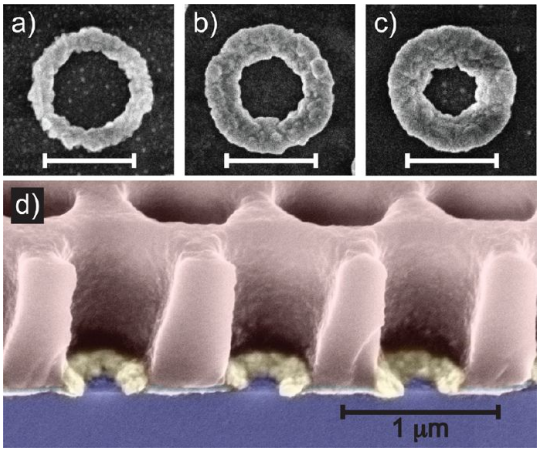

Figure 3. Control of Au nanoring width with increasing deposition time. (a) 300 s and w = 124 nm, (b) 450 s and w = 188 nm (c) 600 s and w = 217 nm. The nanoring radius was constant at 350 nm (scale bar = 500 nm). (d) Cross section of nanoholes with nascent Au nanorings.

spin-coated with a positive photoresist thin film with a thickness of 800 nm. (f) A backside UV exposure of the photoresist was performed *through* the substrate and the nanohole array. (g) The photoresist was developed, revealing an array of cylindrical nanohole band electrodes (either Ni or Ag). (h) A metal (Au, Ag, or Ni) was electrodeposited onto the exposed inner surface of each nanohole electrode to form an array of nanorings. (i) The sacrificial nanohole electrode was selectively removed leaving the nanoring array. For Au or Ag nanorings, the Ni electrode was removed with HNO_3, whereas for Ni nanorings, the Ag electrode was removed with an ammonia etch.

The key step in this fabrication process is the backside exposure of the photoresist through the nanohole array. Backside exposure has been previously used with a negative photoresist to create micrometer-sized rings structures.[54] A similar fabrication technique was described by Ji *et al*., who also used a modified LPNE approach with interference lithography and silicon processing to create arrays of micrometer-sized rings.[55] Our combined approach of LPNE and backside exposure allows us to photopattern and electrodeposit on the submicrometer scale without the need for a high-resolution photomask.

SEM Characterization of the Nanoring Arrays. Using this new LPNE process, a series of gold, silver, and nickel nanoring arrays with different dimensions were fabricated and analyzed with SEM. Some SEM images from a representative gold nanoring array created from a 1 μm colloid monolayer are shown in Figure 2. Each electrodeposited sample had an overall area of 6.25 cm^2; as shown in Figure 2a, these surfaces consisted of multiple 20−30 μm domains of nanoring arrays with an overall colloid to nanoring conversion efficiency of >99%. The vacancies in the array shown in Figure 2a are attributed to imperfections during the self-assembly of the initial colloidal monolayer, not to the subsequent lithographic or electrodeposition steps.

Higher magnification images of the gold nanoring array are shown in Figures 2b and 2c. As seen in these figures, this array retains the initial 1 μm lattice spacing of the colloidal monolayer, but the outer radius of the nanorings have been reduced by the O_2 etching step to approximately 330 $\pm$ 5 nm and the ring width was approximately 135 $\pm$ 4 nm. As seen most strikingly in the SEM image of a single gold nanoring in Figure 2c, the electrodeposited gold nanorings exhibit a significant amount of surface roughness and grain structure. The amount and character of this grain structure depended upon the electrodeposition parameters. The grain size and character of nanowires fabricated by LPNE have been documented previously,[46] and can affect both the electrical and optical properties of the nanorings.

The total cross sectional area of the nanorings could be controlled by the charge passed during electrodeposition. Figure 3a−c shows a series of SEM images of a nanoring with increasing widths from 124, 188, and 217 nm, due to an increase in deposition times from 300, 450, and 600 s, respectively. Unlike the LPNE process for nanowire fabrication that creates a recessed trench for electrodeposition set by the height of the vapor deposited thin film, the metal nanohole film thickness did not control the height of the electrodeposited nanorings. Electrodeposition onto the cylindrical thin film nickel electrode in the nanohole created a roughened, flattened, toroidal nanoring. This unconfined electrodeposition is shown in a cross sectional SEM image before removal of the photoresist (see Figure 1h) in Figure 3d. The SEM image is

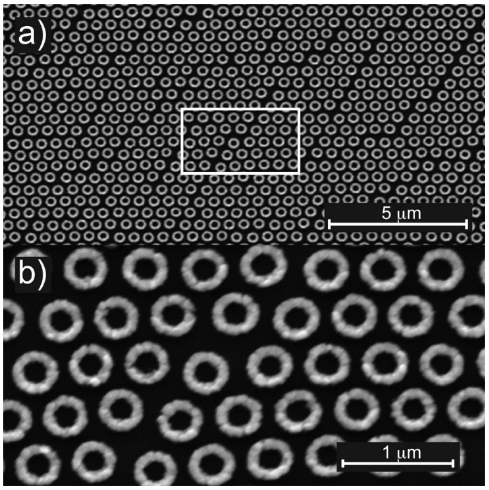

Figure 4. SEM images of Au nanorings fabricated from 0.5 μm colloids. (a) Low and (b) high magnification of nanoring arrays.

displayed in false color: red photoresist, blue glass substrate, yellow nanoring, and gray Ni thin film. The photoresist template generated from the backside lithography process replicated the Ni nanohole with high fidelity and aspect ratio. Additional AFM measurements were used to corroborate that the height was approximately 65% of the nanoring width as shown in the Supporting Information (Figure S1).

The lattice constants of the arrays can also be adjusted by changing the diameter of the initial colloidal monolayer. Figure 4a shows an Au nanoring array fabricated with a 0.5 μm diameter colloidal monolayer and a 70 nm silver sacrificial thin film. In this nanoring array, the dislocations arise during the process of colloidal self-assembly and are more apparent due to the wider distribution of particle diameters. A high magnification SEM image in 4b is used to find and outer radius of 196 $\pm$ 3 nm and width of 93 $\pm$ 3 nm for this nanoring array.

An accurate determination of nanoring size, width, and roughness is necessary for correlation with the optical characteristics of the array. Thus, to characterize the nanoring dimensions, we determined the inner radii (R_{in}) and outer radii (R_{out}) using image processing edge analysis as described in the Supporting Information (Figure S2). For each sample we analyzed over 100 rings, and determined the mean inner, outer radii and width of the ring as well as the Gaussian distribution of the ring roughness, which was found to be approximately 5% of the nanoring width. Some of the data obtained for Au nanoring arrays are shown in Table 1. Starting from the 1 μm colloidal monolayer, we were able vary the radius from 250−400 nm with the O_2 plasma etch time, and widths from 125−225 nm with the charge passed during electrodeposition.

Tunable Nanoring Array NIR Plasmonic Resonance Spectra. Figure 5 shows SEM images and FT-NIR absorption spectra from gold, silver, and nickel nanoring arrays

TABLE 1. Nanoring Dimensions of Samples from Figures 5 and 6

	R_{out} (nm)	σ_{Rout} (nm)	R_{in} (nm)	σ_{Rin} (nm)	w (nm)	σ_w (nm)	ω_{max} (cm^{-1})
Figure 5 samples							
Au	331	4	198	5	133	5	5023
Ag	319	6	179	7	140	4	6134
Ni	375	9	231	10	144	8	4905
Figure 6 samples							
1	401	6	273	7	128	8	3760
2	373	4	250	5	123	5	4095
3	350	4	226	6	124	5	4508
4	331	4	198	5	133	5	5023
5	306	5	172	5	134	4	5558
6	285	7	130	7	155	6	6090

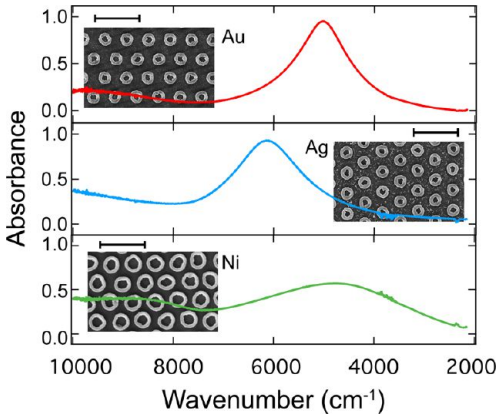

Figure 5. NIR spectra of (a) Au, (b) Ag, and (c) Ni nanoring arrays showing plasmonic resonances in the near-infrared and corresponding SEM images (scale bar = 2 mm).

created by LPNE. The radii and width for the nanorings in these arrays are listed in Table 1. All of the arrays exhibit a strong absorption band in the NIR at 5023, 6134, and 4905 cm^{-1}, respectively. Typically we observe absorbance values around 1 for gold and silver nanoring monolayers and around 0.5 for nickel nanoring monolayers; this corresponded to a coverage of ~10^8 rings/cm^2. The exact position of the absorption band depended upon the metal, the nanoring radius, and the nanoring cross sectional area and have previously been observed for Au and Ag nanorings by several research groups; however, most employ smaller nanorings (diameters below 150 nm) and have resonances at energies above 7000 cm^{-1} (corresponding to wavelengths below 1.4 μm).[3,22,33,38] Lower energy resonances around 5000 cm^{-1}, similar to those observed in this work, have been demonstrated with larger diameter Ag and Au nanorings.[26,44] Although Ni nanorings are primarily studied for their magnetic or magneto-optic properties,[15,18] NIR plasmonic resonances have been observed for Ni nanodisks.[56] In this work, we observe a NIR plasmonic resonance from three different metal nanoring arrays, but note that nanoring array can be fabricated from many other metals and semiconductors with the LPNE approach.[47]

The position of the NIR plasmonic resonance could be tuned by varying the nanoring radius with the plasma etching time. As an example, Figure 6 shows a series of NIR spectra acquired from a set of Au nanorings arrays created by varying the plasma etch time from 240 to 360 s and fixing the electrodeposition time at 300 s. The peak positions of these NIR spectra varied from 3760 to 6090 cm^{-1} and are listed as ω_{max} in Table 1. Above the spectra in the figure are a set of corresponding SEM images of single exemplary nanorings. Analysis of these SEM images revealed that the outer radii of the nanorings varied systematically from 285 to 400 nm, while the nanoring width was kept relatively constant at 125−155 nm (see Table 1).

The position of the NIR plasmonic resonance in wavelength (λ_{max}) varied linearly with the outer radius of nanorings in the array. Figure 7a plots λ_{max} *versus* the outer radius (R_{out}) of the gold nanorings created with a 300 s electrodeposition time (black circles). Also plotted in Figure 7a are the λ_{max} *versus* R_{out} plots for thicker nanoring arrays created by varying the plasma etch time and fixing the electrodeposition time to either 450 s (blue) or 600 s (green). In each case, a linear relationship was observed between λ_{max} and R_{out}. This has been seen previously in nanoring arrays

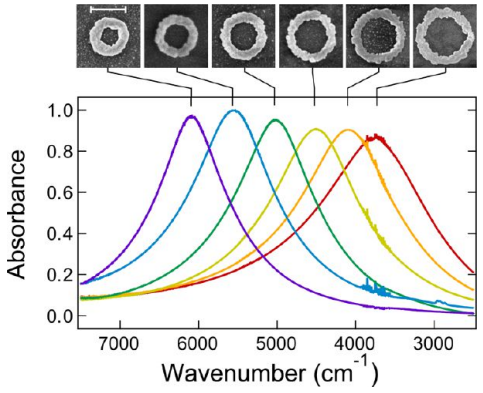

Figure 6. NIR spectra of Au ring resonance with varying radius. Each spectrum is shown with its corresponding SEM of a single nanoring from the array (scale bar = 500 nm).

by other research groups and has been explained using a simple standing wave model optical antenna theory[57] that uses an effective antenna length for nanoring and split-ring systems.[44,58]

The data for the gold nanoring arrays in Figure 7a are replotted in Figure 7b as the NIR plasmonic resonance frequency (ω_{max}, in cm^{-1}) *versus* the radius/width ratio (R_{out}/w) (red circles). The data from the three electrodeposition times (300, 450, 600 s) all fall on an approximately straight line with a slope of −1945 cm^{-1}. Also plotted in Figure 7b are data sets of from both Ag and Ni nanoring arrays; the same behavior is observed as in the case of the Au nanorings, but with different slopes of −1475 and −3350 cm^{-1}, respectively. The parameter of nanoring width/radius has been used previously to describe observed variations of ω_{max} for sets of small nanorings (<200 nm) using a variety of theories including the Mie theory of spherical particles,[22] and plasmon hybridization.[23] These calculations use a Drude model for the metal dielectric function and describe a tunable dipolar resonance that varies from zero to the surface plasmon frequency ω_{sp} as the nanoring width/radius ratio varies from zero to 1. The results in Figure 7b cannot be quantitatively fit with these theories; we attribute this discrepancy to a combination of (i) the roughness of the electrodeposited nanorings, (ii) the noncylindrical nanoring cross section, and (iii) the coupling of the nanorings in the close-packed arrays.[37,44] Nevertheless, the observation of three different slopes in Figure 7b for the gold, nickel, and silver nanoring arrays does imply that the metal complex dielectric susceptibility does control the position of the NIR plasmonic resonances in these systems.

Double Nanoring Arrays. A significant advantage of the nanoring array electrodeposition method described in this paper is its ability to create more intricate structures from a range of different materials. Concentric nanorings are one such structure, and they are potentially useful for sensing applications by utilizing Fano resonances or the enhanced fields in the gap

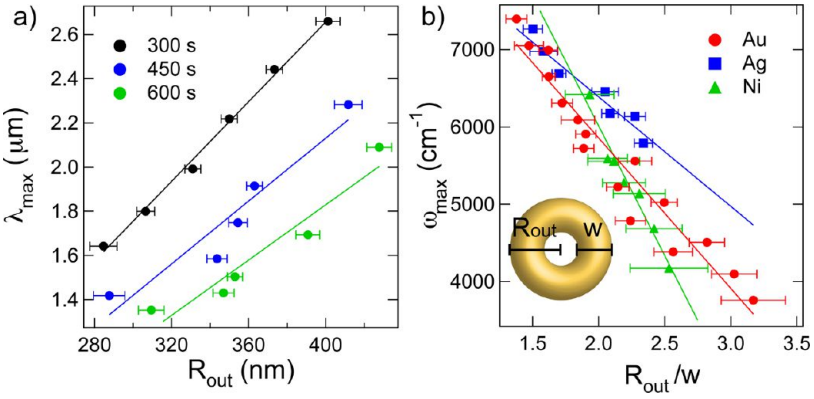

Figure 7. (a) Au nanorings resonance wavelength (λ_{max}) dependence on outer radius for fixed electrodeposition times. (b) Gold, silver, and nickel resonance wavenumber (ω_{max}) dependence on radius/width ratio.

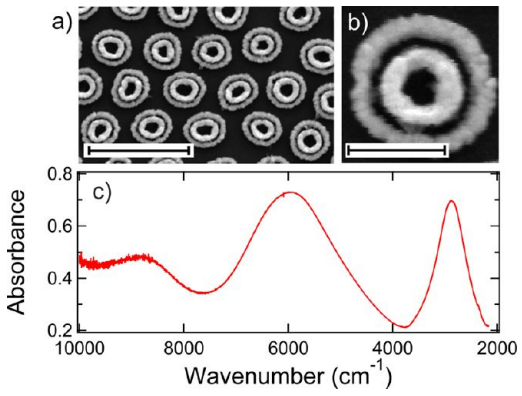

Figure 8. Concentric nanoring arrays characterization. (a) SEM image of an array of concentric nanorings (scale bar = 2 μm), and (b) single concentric nanoring (scale bar = 500 nm). (c) NIR spectrum of concentric nanoring showing two resonances.

region.[4,43,59,60] Other methods exist for generating concentric gold ring arrays including a three-step edge spreading lithography process,[40] block copolymers templates,[61] or by ion etching nanopillars laminated by gold thin films.[43] Using our LPNE nanoring fabrication process, the formation of bimetallic rings or concentric rings is easily accomplished through the use of multiple electrodeposition steps. SEM images of an array of two concentric gold nanorings created by a multistep, bimetallic, nanoscale electrodeposition process are shown in Figure 8a,b. Construction of the concentric gold nanorings was accomplished by forgoing the final sacrificial electrode removal step (Figure 1i) and repeating steps in Figure 1e−h twice to create three concentric nanorings of gold, nickel, and gold. Removal of the sacrificial Ni electrode by wet etching also removed the sandwiched nickel ring, leaving two concentric gold nanorings. The outer nanoring had a radius and width of 396 and 108 nm, and the inner nanoring had a radius and width of 247 and 125 nm. Owing to the nature of the electrodeposition process, the nanohole wall height increased, causing the inner ring to become taller than the outer ring. This height differences caused the inner ring to appear brighter in the SEM image; and was confirmed by AFM to be about 85 nm taller.

The NIR spectra of the double gold nanoring array is shown in Figure 8c. The double rings result in two peaks in the NIR spectra at 2790 and 5960 cm^{-1}. The peak width of the low energy resonance is much narrower than the spectra for single rings. This behavior has been designated as a coupling effect for similar ring/disk nanocavities.[60,62] Additionally, there is a small peak at 9000 cm^{-1} that we assign to a quadrupolar resonance that is more prominent in the double nanoring array.[26]

CONCLUSIONS

In this paper we have described a simple yet versatile approach for the lithographically patterned electrodeposition of close-packed arrays of metallic nanorings. A combination of colloidal lithography and LPNE was employed; the critical step in this fabrication process was the formation of an array of cylindrical nanoscale electrodes by the backside exposure of a thin film of photoresist through a nanohole array. The resultant electrodeposited gold, silver, and nickel nanoring arrays displayed NIR plasmonic resonances that could be tuned from 3500 to 8000 cm^{-1} by changing the radius and width of the nanorings during the fabrication process. We have created nanoring arrays from three plasmonic metals (Au, Ag, and Ni), but intend to apply this process in future efforts to other LPNE compatible metals (*e.g.*, Pt, Pd, Bi), semiconductors (*e.g.*, CdSe, PbTe), and conductive polymers (*e.g.*, PEDOT). The fabrication process was also extended to include multiple electrodeposition steps to create more complex concentric ring structures that show multiple NIR resonances; this opens up the possibility to create a variety of bimetallic, trimetallic, and metal/semiconductor nanoring arrays with potential applications in the fabrication of plasmonic antennae, plasmonic semiconductors, and negative index metamaterials.

EXPERIMENTAL SECTION

Materials. Polystyrene beads solutions (2.6% w/v, 1 or 0.5 μm diameter, carboxylate coated) were purchased from Polysciences (Warrington, PA). Shipley S1808 photoresist, Thinner P, and MF-319 developer were purchased from Microchem (Newton, MA). Clean Earth Chemicals Silver and 24K gold plating solutions (Grobet USA, Carlstadt, NJ) were used as received. Fisher Premium glass microscope slides (1 mm thick) were used as substrates.

Colloidal Monolayer Self-Assembly. The stock solution of polystyrene beads was concentrated to 5.2% w/v containing 75% methanol by volume. Hydrophilic oxygen plasma cleaned microscope slides were cut to 2.5 cm squares, and spin coated at 1000 rpm (4000 rpm for 0.5 μm) for 6 s with 10−15 μL of the bead solution. It was necessary to fine-tune the spin and drying conditions to form well-packed monolayers. Once dry, the beads were etched in an oxygen plasma (200 mTorr, 50 W, −400 VDC, South Bay Technologies, San Clemente, CA) for 240−360 s (60−180 s for 0.5 μm).

Nanoring Electrode Array Fabrication. A 70 nm layer of Ni was vapor deposited on top of the etched beads by thermal evaporation. For Ag layers, an initial 1 nm Cr adhesion layer was used. The beads were removed by sonication in toluene to create the nanohole array. Shipley S1808 photoresist was spin coated on the 1 μm lattice constant nanohole arrays (80 s, 2500 rpm) and baked for 30 min at 90 °C. For 500 nm lattice constant arrays, a 1:1 solution of S1808 to Thinner P was used. The photoresist was backside exposed through the nanohole array with ~60 mW/cm^2 (or 30 mw/cm^2 for the 1:1 dilution), and developed with MF-319.

Nanoring Electrodeposition. A potentiostat (PGSTAT12, Metrohm, Riverview, FL) and an Ag/AgCl reference electrode were used to control the electrodepostion. Au rings were deposited inside Ni nanoholes for 300−600 s at −0.85 V using a 24K gold plating

solution. Likewise, Ag rings were deposited inside Ni nanoholes at −0.1 V for 150 s, following a −1 V pulse for 0.75 s using a silver plating solution. Ni rings were deposited inside Ag nanoholes at −0.85 V for 600 s using a Ni plating solution (5 mM $NiCl_2$, 5 mM boric acid, 0.1 M KCl). Ni sacrificial electrodes were removed with 0.8 M HNO_3 and Ag was removed with a 5% NH_4OH and 1% H_2O_2 solution.

SEM and AFM Measurements. Nanorings width measurements were performed using SEM images acquired on a FEI Magellan. AFM height measurements were taken on an Asylum MFP-3D.

FT-NIR Absorption Spectra. A Mattson RS-1 FTIR with a halogen source, CaF_2 beamsplitter and InSb detector was used to capture NIR spectra from 2000−10000 cm^{-1}. The beam was focused to ~3 mm in diameter to interrogate different areas of the sample. A bare glass slide was used as a reference spectrum to subtract off the silica absorption below 3500 cm^{-1}.

Conflict of Interest: The authors declare no competing financial interest.

Acknowledgment. This work is supported by the National Science Foundation through CHE-1057638. The authors thank Prof. R. Penner for access to his laboratory and for helpful discussions.

Supporting Information Available: Additional figures as described in the text. This material is available free of charge *via* the Internet at http://pubs.acs.org.

REFERENCES AND NOTES

1. Nordlander, P. The Ring: A Leitmotif in Plasmonics. *ACS Nano* **2009**, *3*, 488–492.
2. Kim, S.; Jung, J. M.; Choi, D. G.; Jung, H. T.; Yang, S. M. Patterned Arrays of Au Rings for Localized Surface Plasmon Resonance. *Langmuir* **2006**, *22*, 7109–7112.
3. Larsson, E. M.; Alegret, J.; Kall, M.; Sutherland, D. S. Sensing Characteristics of NIR Localized Surface Plasmon Resonances in Gold Nanorings for Application as Ultrasensitive Biosensors. *Nano Lett.* **2007**, *7*, 1256–1263.
4. Cetin, A. E.; Altug, H. Fano Resonant Ring/Disk Plasmonic Nanocavities on Conducting Substrates for Advanced Biosensing. *ACS Nano* **2012**, *6*, 9989–9995.
5. Huang, C. J.; Ye, J.; Wang, S.; Stakenborg, T.; Lagae, L. Gold Nanoring as a Sensitive Plasmonic Biosensor for on-Chip DNA Detection. *Appl. Phys. Lett.* **2012**, *100*, 173114.
6. Clark, A. W.; Glidle, A.; Cumming, D. R. S.; Cooper, J. M. Plasmonic Split-Ring Resonators as Dichroic Nanophotonic DNA Biosensors. *J. Am. Chem. Soc.* **2009**, *131*, 17615–17619.
7. Clark, A. W.; Sheridan, A. K.; Glidle, A.; Cumming, D. R. S.; Cooper, J. M. Tuneable Visible Resonances in Crescent Shaped Nano-Split-Ring Resonators. *Appl. Phys. Lett.* **2007**, *91*, 093109.
8. Gwinner, M. C.; Koroknay, E.; Fu, L. W.; Patoka, P.; Kandulski, W.; Giersig, M.; Giessen, H. Periodic Large-Area Metallic Split-Ring Resonator Metamaterial Fabrication Based on Shadow Nanosphere Lithography. *Small* **2009**, *5*, 400–406.
9. Cataldo, S.; Zhao, J.; Neubrech, F.; Frank, B.; Zhang, C. J.; Braun, P. V.; Giessen, H. Hole-Mask Colloidal Nanolithography for Large-Area Low-Cost Metamaterials and Antenna-Assisted Surface-Enhanced Infrared Absorption Substrates. *ACS Nano* **2012**, *6*, 979–985.
10. Babayan, Y.; McMahon, J. M.; Li, S. Z.; Gray, S. K.; Schatz, G. C.; Odom, T. W. Confining Standing Waves in Optical Corrals. *ACS Nano* **2009**, *3*, 615–620.
11. Jung, K. Y.; Teixeira, F. L.; Reano, R. M. Au/SiO_2 Nanoring Plasmon Waveguides at Optical Communication Band. *J. Lightwave Technol.* **2007**, *25*, 2757–2765.
12. Kosiorek, A.; Kandulski, W.; Glaczynska, H.; Giersig, M. Fabrication of Nanoscale Rings, Dots, and Rods by Combining Shadow Nanosphere Lithography and Annealed Polystyrene Nanosphere Masks. *Small* **2005**, *1*, 439–444.
13. Duan, G. T.; Cai, W. P.; Luo, Y. Y.; Li, Z. G.; Lei, Y. Hierarchical Structured Ni Nanoring and Hollow Sphere Arrays by Morphology Inheritance Based on Ordered through-Pore Template and Electrodeposition. *J. Phys. Chem. B* **2006**, *110*, 15729–15733.
14. Wang, S.; Yu, G. J.; Gong, J. L.; Li, Q. T.; Xu, H. J.; Zhu, D. Z.; Zhu, Z. Y. Large-Area Fabrication of Periodic Fe Nanorings with Controllable Aspect Ratios in Porous Alumina Templates. *Nanotechnology* **2006**, *17*, 1594–1598.
15. Ren, Y.; Adeyeye, A. O.; Nam, C.; Ross, C. A. Effects of Interlayer Coupling in Elongated Ni80Fe20/Au/Co Nanorings. *IEEE. Trans. Magn.* **2010**, *46*, 1906–1909.
16. Li, Y. L.; Tang, S. L.; Xia, W. B.; Chen, L. Y.; Wang, Y.; Tang, T.; Du, Y. W. Large Area Co Nanoring Arrays Fabricated on Silicon Substrate by Anodic Aluminum Oxide Template-Assisted Electrodeposition. *Appl. Phys. Lett.* **2012**, *100*, 183101.
17. Li, Z. G.; Liu, P. S.; Liu, Y. P.; Chen, W. P.; Wang, G. P. Fabrication of Size-Controllable Fe_2O_3 Nanoring Array *via* Colloidal Lithography. *Nanoscale* **2011**, *3*, 2743–2747.
18. Wang, Z. K.; Lim, H. S.; Liu, H. Y.; Ng, S. C.; Kuok, M. H.; Tay, L. L.; Lockwood, D. J.; Cottam, M. G.; Hobbs, K. L.; Larson, P. R.; *et al.* Spin Waves in Nickel Nanorings of Large Aspect Ratio. *Phys. Rev. Lett.* **2005**, *94*, 137208.
19. Chen, J. X.; Liao, W. S.; Chen, X.; Yang, T. L.; Wark, S. E.; Son, D. H.; Batteas, J. D.; Cremer, P. S. Evaporation-Induced Assembly of Quantum Dots into Nanorings. *ACS Nano* **2009**, *3*, 173–180.
20. Li, K. H.; Ma, Z. T.; Choi, H. W. High-Q Whispering-Gallery Mode Lasing from Nanosphere-Patterned GaN Nanoring Arrays. *Appl. Phys. Lett.* **2011**, *98*, 071106.
21. Lorke, A.; Luyken, R. J.; Govorov, A. O.; Kotthaus, J. P.; Garcia, J. M.; Petroff, P. M. Spectroscopy of Nanoscopic Semiconductor Rings. *Phys. Rev. Lett.* **2000**, *84*, 2223–2226.
22. Aizpurua, J.; Hanarp, P.; Sutherland, D. S.; Kall, M.; Bryant, G. W.; de Abajo, F. J. G. Optical Properties of Gold Nanorings. *Phys. Rev. Lett.* **2003**, *90*, 057401.
23. Dutta, C. M.; Ali, T. A.; Brandl, D. W.; Park, T. H.; Nordlander, P. Plasmonic Properties of a Metallic Torus. *J. Chem. Phys.* **2008**, *129*, 084706.
24. Prodan, E.; Radloff, C.; Halas, N. J.; Nordlander, P. A Hybridization Model for the Plasmon Response of Complex Nanostructures. *Science* **2003**, *302*, 419–422.
25. Mary, A.; Koller, D. M.; Hohenau, A.; Krenn, J. R.; Bouhelier, A.; Dereux, A. Optical Absorption of Torus-Shaped Metal Nanoparticles in the Visible Range. *Phys. Rev. B* **2007**, *76*.
26. Hao, F.; Larsson, E. M.; Ali, T. A.; Sutherland, D. S.; Nordlander, P. Shedding Light on Dark Plasmons in Gold Nanorings. *Chem. Phys. Lett.* **2008**, *458*, 262–266.
27. Hulteen, J. C.; Van Duyne, R. P. Nanosphere Lithography: A Materials General Fabrication Process For Periodic Particle Aarray Surfaces. *J. Vac. Sci. Technol. A* **1995**, *13*, 1553–1558.
28. Winzer, M.; Kleiber, M.; Dix, N.; Wiesendanger, R. Fabrication of Nano-Dot- and Nano-Ring-Arrays by Nanosphere Lithography. *Appl. Phys. A-Mater.* **1996**, *63*, 617–619.
29. Hanarp, P.; Kall, M.; Sutherland, D. S. Optical Properties of Short Range Ordered Arrays of Nanometer Gold Disks Prepared by Colloidal Lithography. *J. Phys. Chem. B* **2003**, *107*, 5768–5772.
30. Langhammer, C.; Yuan, Z.; Zoric, I.; Kasemo, B. Plasmonic Properties of Supported Pt and Pd Nanostructures. *Nano Lett.* **2006**, *6*, 833–838.
31. Shumaker-Parry, J. S.; Rochholz, H.; Kreiter, M. Fabrication of Crescent-Shaped Optical Antennas. *Adv. Mater.* **2005**, *17*, 2131–2134.
32. Bukasov, R.; Shumaker-Parry, J. S. Highly Tunable Infrared Extinction Properties of Gold Nanocrescents. *Nano Lett.* **2007**, *7*, 1113–1118.
33. Banaee, M. G.; Crozier, K. B. Gold Nanorings as Substrates for Surface-Enhanced Raman Scattering. *Opt. Lett.* **2010**, *35*, 760–762.
34. Tsai, C. Y.; Lu, S. P.; Lin, J. W.; Lee, P. T. High Sensitivity Plasmonic Index Sensor Using Slablike Gold Nanoring Arrays. *Appl. Phys. Lett.* **2011**, *98*, 153108.
35. Near, R.; Tabor, C.; Duan, J. S.; Pachter, R.; El-Sayed, M. Pronounced Effects of Anisotropy on Plasmonic Properties of Nanorings Fabricated by Electron Beam Lithography. *Nano Lett.* **2012**, *12*, 2158–2164.

36. Lehr, D.; Dietrich, K.; Helgert, C.; Kasebier, T.; Fuchs, H. J.; Tunnermann, A.; Kley, E. B. Plasmonic Properties of Aluminum Nanorings Generated by Double Patterning. *Opt. Lett.* **2012**, *37*, 157–159.
37. Jiang, H.; Sabarinathan, J. Effects of Coherent Interactions on the Sensing Characteristics of Near-Infrared Gold Nanorings. *J. Phys. Chem. C* **2010**, *114*, 15243–15250.
38. Ye, J.; Van Dorpe, P.; Lagae, L.; Maes, G.; Borghs, G. Observation of Plasmonic Dipolar Anti-Bonding Mode in Silver Nanoring Structures. *Nanotechnology* **2009**, *20*.
39. McLellan, J. M.; Geissler, M.; Xia, Y. N. Edge Spreading Lithography and Its Application to the Fabrication of Mesoscopic Gold and Silver Rings. *J. Am. Chem. Soc.* **2004**, *126*, 10830–10831.
40. Geissler, M.; McLellan, J. M.; Chen, J. Y.; Xia, Y. N. Side-by-Side Patterning of Multiple Alkanethiolate Monolayers on Gold by Edge-Spreading Lithography. *Angew. Chem., Int. Ed.* **2005**, *44*, 3596–3600.
41. Yan, F.; Goedel, W. A. Preparation of Mesoscopic Gold Rings Using Particle Imprinted Templates. *Nano Lett.* **2004**, *4*, 1193–1196.
42. Lusker, K. L.; Li, J. R.; Garno, J. C. Nanostructures of Functionalized Gold Nanoparticles Prepared by Particle Lithography with Organosilanes. *Langmuir* **2011**, *27*, 13269–13275.
43. Kubo, W.; Fujikawa, S. Au Double Nanopillars with Nanogap for Plasmonic Sensor. *Nano Lett.* **2011**, *11*, 8–15.
44. Cai, Y. J.; Li, Y.; Nordlander, P.; Cremer, P. S. Fabrication of Elliptical Nanorings with Highly Tunable and Multiple Plasmonic Resonances. *Nano Lett.* **2012**, *12*, 4881–4888.
45. Menke, E. J.; Thompson, M. A.; Xiang, C.; Yang, L. C.; Penner, R. M. Lithographically Patterned Nanowire Electrodeposition. *Nat. Mater.* **2006**, *5*, 914–919.
46. Xiang, C. X.; Kung, S. C.; Taggart, D. K.; Yang, F.; Thompson, M. A.; Guell, A. G.; Yang, Y. A.; Penner, R. M. Lithographically Patterned Nanowire Electrodeposition: A Method for Patterning Electrically Continuous Metal Nanowires on Dielectrics. *ACS Nano* **2008**, *2*, 1939–1949.
47. Xiang, C. X.; Yang, Y. G.; Penner, R. M. Cheating the Diffraction Limit: Electrodeposited Nanowires Patterned by Photolithography. *Chem. Commun.* **2009**, 859–873.
48. Yang, Y. A.; Kung, S. C.; Taggart, D. K.; Xiang, C.; Yang, F.; Brown, M. A.; Guell, A. G.; Kruse, T. J.; Hemminger, J. C.; Penner, R. M. Synthesis of PbTe Nanowire Arrays Using Lithographically Patterned Nanowire Electrodeposition. *Nano Lett.* **2008**, *8*, 2447–2451.
49. Kung, S. C.; van der Veer, W. E.; Yang, F.; Donavan, K. C.; Penner, R. M. 20 μs Photocurrent Response from Lithographically Patterned Nanocrystalline Cadmium Selenide Nanowires. *Nano Lett.* **2010**, *10*, 1481–1485.
50. Arter, J. A.; Taggart, D. K.; McIntire, T. M.; Penner, R. M.; Weiss, G. A. Virus-PEDOT Nanowires for Biosensing. *Nano Lett.* **2010**, *10*, 4858–4862.
51. Ctistis, G.; Patoka, P.; Wang, X.; Kempa, K.; Giersig, M. Optical Transmission through Hexagonal Arrays of Subwavelength Holes in Thin Metal Films. *Nano Lett.* **2007**, *7*, 2926–2930.
52. Jiang, P.; McFarland, M. J. Wafer-Scale Periodic Nanohole Arrays Templated from Two-Dimensional Nonclose-Packed Colloidal Crystals. *J. Am. Chem. Soc.* **2005**, *127*, 3710–3711.
53. Canpean, V.; Astilean, S. Extending Nanosphere Lithography for the Fabrication of Periodic Arrays of Subwavelength Metallic Nanoholes. *Mater. Lett.* **2009**, *63*, 2520–2522.
54. Gottron, N. J.; Yellen, B. B. Self-Aligned Reduction Lithography Using Backside Exposure through Embedded Masks. *J. Micromech. Microeng.* **2011**, *21*, 075022.
55. Ji, R.; Lee, W.; Scholz, R.; Gosele, U.; Nielsch, K. Templated Fabrication of Nanowire and Nanoring Arrays Based on Interference Lithography and Electrochemical Deposition. *Adv. Mater.* **2006**, *18*, 2593–2596.
56. Chen, J. N.; Albella, P.; Pirzadeh, Z.; Alonso-Gonzalez, P.; Huth, F.; Bonetti, S.; Bonanni, V.; Akerman, J.; Nogues, J.; Vavassori, P.; *et al.* Plasmonic Nickel Nanoantennas. *Small* **2011**, *7*, 2341–2347.
57. Novotny, L. Effective Wavelength Scaling for Optical Antennas. *Phys. Rev. Lett.* **2007**, *98*, 266802.
58. Chen, C. Y.; Wu, S. C.; Yen, T. J. Experimental Verification of Standing-Wave Plasmonic Resonances in Split-Ring Resonators. *Appl. Phys. Lett.* **2008**, *93*, 034110.
59. Liu, S. D.; Yang, Z.; Liu, R. P.; Li, X. Y. High Sensitivity Localized Surface Plasmon Resonance Sensing Using a Double Split NanoRing Cavity. *J. Phys. Chem. C* **2011**, *115*, 24469–24477.
60. Hao, F.; Nordlander, P.; Sonnefraud, Y.; Van Dorpe, P.; Maier, S. A. Tunability of Subradiant Dipolar and Fano-Type Plasmon Resonances in Metallic Ring/Disk Cavities: Implications for Nanoscale Optical Sensing. *ACS Nano* **2009**, *3*, 643–652.
61. Chai, J.; Buriak, J. M. Using Cylindrical Domains of Block Copolymers to Self-Assemble and Align Metallic Nanowires. *ACS Nano* **2008**, *2*, 489–501.
62. Hao, F.; Nordlander, P.; Burnett, M. T.; Maier, S. A. Enhanced Tunability and Linewidth Sharpening of Plasmon Resonances in Hybridized Metallic Ring/Disk Nanocavities. *Phys. Rev. B* **2007**, *76*, 245417.